The Journal of Molecular Diagnostics, Vol. 25, No. 10, October 2023

ELSEVIER

the Journal of Molecular Diagnostics
jmdjournal.org

Formalin-Fixed, Paraffin-Embedded—Targeted Locus Capture

A Next-Generation Sequencing Technology for Accurate DNA-Based Gene Fusion Detection in Bone and Soft Tissue Tumors

Ellen Stelloo,* Ruud W.J. Meijers,† Joost F. Swennenhuis,* Amin Allahyar,‡ Karima Hajo,* Mario Cangiano,* Wendy W.J. de Leng,† Sjoerd van Helvert,§ Joni Van der Meulen,¶ David Creytens,‖ Léon C. van Kempen,**†† Anne-Marie Cleton-Jansen,‡‡ Judith V.M.G. Bovee,‡‡ Wouter de Laat,‡ Erik Splinter,* and Harma Feitsma*

From Cergentis BV, Utrecht, the Netherlands; the Department of Pathology,† University Medical Center Utrecht, Utrecht, the Netherlands; the Oncode Institute,‡ Hubrecht Institute—Royal Netherlands Academy of Arts and Sciences, and University Medical Center Utrecht, Utrecht, the Netherlands; the Department of Pathology,§ Radboud University Medical Center, Nijmegen, the Netherlands; Molecular Diagnostics¶ and the Department of Pathology,‖ Ghent University Hospital, Ghent, Belgium; the Department of Pathology,** University Hospital Antwerp, University of Antwerp, Antwerp, Belgium; the Department of Pathology and Medical Biology,†† University Medical Center Groningen, University of Groningen, Groningen, the Netherlands; and the Department of Pathology,‡‡ Leiden University Medical Center, Leiden, the Netherlands*

Accepted for publication June 28, 2023.

Address correspondence to Harma Feitsma, Ph.D., Cergentis BV, Yalelaan 62, 3584 CM Utrecht, the Netherlands. E-mail: harma.feitsma@cergentis.com.

Chromosomal rearrangements are important drivers in cancer, and their robust detection is essential for diagnosis, prognosis, and treatment selection, particularly for bone and soft tissue tumors. Current diagnostic methods are hindered by limitations, including difficulties with multiplexing targets and poor quality of RNA. A novel targeted DNA-based next-generation sequencing method, formalin-fixed, paraffin-embedded—targeted locus capture (FFPE-TLC), has shown advantages over current diagnostic methods when applied on FFPE lymphomas, including the ability to detect novel rearrangements. We evaluated the utility of FFPE-TLC in bone and soft tissue tumor diagnostics. FFPE-TLC sequencing was successfully applied on noncalcified and decalcified FFPE samples ($n = 44$) and control samples ($n = 19$). In total, 58 rearrangements were identified in 40 FFPE tumor samples, including three previously negative samples, and none was identified in the FFPE control samples. In all five discordant cases, FFPE-TLC could identify gene fusions where other methods had failed due to either detection limits or poor sample quality. FFPE-TLC achieved a high specificity and sensitivity (no false positives and negatives). These results indicate that FFPE-TLC is applicable in cancer diagnostics to simultaneously analyze many genes for their involvement in gene fusions. Similar to the observation in lymphomas, FFPE-TLC is a good DNA-based alternative to the conventional methods for detection of rearrangements in bone and soft tissue tumors. *(J Mol Diagn 2023, 25: 758—770; https://doi.org/10.1016/j.jmoldx.2023.06.012)*

Bone and soft tissue tumors comprise a large and heterogeneous group of mesenchymal neoplasms that are known to have >150 different subtypes.[1] Many types of bone and soft tissue tumors are characterized by fusion genes generated through chromosomal rearrangements as potential drivers. Over the past several years, identification of such rearrangements has shown that these tumors are genetically diverse, with new rearrangements still being identified, contributing to better diagnosis.[2] Increased molecular

Supported by Dutch Cancer Society/Alpe project 11632/2018-1 and Oncode Institute (work conducted by A.A. and W.d.L. at the Hubrecht Institute).

Disclosures: J.F.S., E.St., K.H., M.C., H.F., and E.Sp. are Cergentis BV employees. The other authors declare no competing interests.

https://doi.org/10.1016/j.jmoldx.2023.06.012

knowledge may reduce the diagnostic uncertainty, leading to better stratifications for treatment, prognosis predictions, and novel therapeutics for bone and soft tissue tumors.[3–5]

Conventional techniques used for rearrangement detection in formalin-fixed, paraffin-embedded (FFPE) specimens include (break-apart and fusion) fluorescence *in situ* hybridization (FISH) and RT-PCR.[6] Recently, high-throughput multiplex RNA techniques are often being introduced in routine diagnostics.[7–10] Although commonly used, several limitations of these techniques are known. For example, as FISH and RT-PCR are single-target assays and there is high variability of rearrangements in bone and soft tissue tumors, diagnosis often requires multiple consecutive analyses. In addition, reliable interpretation of break-apart FISH is dependent on good tissue morphology and clear FISH signals, which might be challenging in case of uncommon breakpoints or copy number variations.[11] Also, break-apart FISH does not provide information about the fusion gene partner. RT-PCR and high-throughput multiplex RNA technologies require that the RNA quality is sufficiently preserved, which is not always the case in FFPE samples as formalin fixation induces RNA (and DNA) fragmentation.[12] Also, as with FISH, fusions might be missed if the breakpoint or fusion partner has not been previously described or in case of a fusion within noncoding sequences (ie, such as regulatory elements).[13–16]

As DNA is more stable than RNA, rearrangement detection by targeted DNA-based next-generation sequencing (NGS) methods is a good alternative for FFPE specimens, allowing for the identification of breakpoints, gene fusion partners, and other structural variants.[17,18] However, detection of intronic breakpoints, especially located in repetitive regions, is a challenge for these methods,[18] and those fusions may be missed.

Proximity-ligation methods have shown to be a powerful method for rearrangement detection,[19–21] and FFPE-targeted locus capture (TLC) was recently demonstrated to be a robust and accurate method for rearrangement detection in lymphomas.[22] FFPE-TLC is based on the cross-linking and fragmentation of DNA, and therefore is particularly suitable for the analysis of FFPE samples in which DNA is inherently cross-linked and fragmented. These cross-linked DNA fragments, which are in close proximity in the three-dimensional nuclear space, are *in situ* ligated, followed by conventional target enrichment using oligonucleotide probe sets to selectively pull down, sequence, and analyze proximity-ligation products of selected clinically relevant genes (Supplemental Figure S1). Sequencing data collected with this method can be processed automatedly for rearrangement detection, and both familiar and previously unidentified rearrangement partners can be identified by FFPE-TLC.[22] The data showed that FFPE-TLC outperformed FISH, currently still the gold standard for rearrangement detection in lymphomas,[22] for both sensitivity and specificity. Compared with conventional (targeted) NGS methods, FFPE-TLC offers the advantage that it does not only rely on the capturing and sequencing of fusion reads for the detection of chromosomal rearrangements, but that it also identifies them based on significant accumulation of proximity-ligation events at the fusion partner. This enables detection of gene fusions even if probes are not targeting the exact fusion sequences and when nonunique sequences flank the rearrangement breakpoint.[22]

Here, we investigated the utility of FFPE-TLC for the detection of rearrangements in FFPE samples of solid tumors other than lymphoma. For this, a custom gene panel was designed targeting 49 genes associated with gene fusions and bone and soft tissue tumors. In total, 44 bone and soft tissue tumor samples and 19 control samples from five participating centers were collected and analyzed. The outcome of FFPE-TLC sequencing was compared with the outcome of the standard fusion gene detection method used in each participating center. The data demonstrate that FFPE-TLC is a powerful method for the detection and characterization of clinically relevant rearrangements in different types of FFPE solid tumor samples.

Materials and Methods

The methods describe the processing of FFPE tissue to restricted and vicinity religated DNA fragments by making use of the formalin fixation during the paraffin-embedding process. The tissue is first pretreated such that the DNA is accessible for enzymes while enough cross-links remain to promote vicinity ligation. The processes following these FFPE-TLC–specific steps are standard library preparation, hybrid-capture, and paired-end sequencing. The main element of the data analysis pipeline, proximity-ligation–based identification of rearrangements (PLIER), identifies genomic regions where reads are linked to specific targeted genes. These regions are subsequently visualized in butterfly plots, heat map representations of the sequence products spanning chromosomal rearrangement breakpoints.

Archival FFPE Tissue Samples

A total of 63 FFPE samples were randomly selected from the archives of five participating centers: Leiden University Medical Center (Leiden, the Netherlands), University Medical Center Groningen (Groningen, the Netherlands), University Medical Center Utrecht (Utrecht, the Netherlands), Ghent University Hospital (Ghent, Belgium), and Radboud University Medical Center (Nijmegen, the Netherlands). This included 44 FFPE samples of patients diagnosed with bone and soft tissue tumors between 2014 and 2021 and 19 control FFPE samples from bone, tonsil, and nonreactive lymph nodes. The study was performed in accordance with the local institutional board requirements, and all relevant ethical and privacy regulations were followed during this study. The use of tissue specimens and associated data in this study was approved by the TcBio of

University Medical Center Utrecht as gebruik van restmateriaal, the human research committee of Radboud University Medical Center (case number 2021-13004), the Ethics Committee of Ghent University Hospital (project 2004/094), the Medical Ethical Committee of University Medical Center Groningen for explorative research with anonymized leftover tissues, and the Medical Ethical Committee of Leiden University Medical Center under code of conduct of secondary use of tissues.

FFPE-TLC Library Preparation

FFPE-TLC was performed on one to three unstained FFPE tissue slides or scrolls (4 to 10 μm thick), as previously described[22] (Supplemental Figure S1 and Figure 1, A and B). Briefly, excessive paraffin from the scraped material or scrolls was first removed by incubation in a 1.5 mL Eppendorf tube in 1× CutSmart buffer (New England Biolabs, Ipswich, MA) containing 0.02% Igepal (Sigma Aldrich, St. Louis, MO) at 80°C for 3 minutes. After 1-minute centrifugation at 20,000 × *g*, the solidified layer of paraffin on the top was carefully removed. Tissue was transferred to a 130-μL Covaris tube (Covaris, LLC, Woburn, MA) and sonified on a M220 Covaris machine for 300 seconds (duty factor, 10%; power, 75 W; 200 cycles/burst at 20°C). Then, after transfer to a 1.5-mL Eppendorf tube, tissues were permeabilized with 0.3% SDS at 90°C for 30 minutes and neutralized with 2.5% final concentration EcoSurf SA9 (Sigma Aldrich) for 10 minutes at 37°C. This was followed by digestion with restriction enzyme NlaIII at 37°C for 1 hour and ligation with T4 DNA ligase at room temperature for 2 hours. NlaIII is a 4-bp cutter restriction enzyme, which cuts every approximately 250 to 500 bp in the genome. Next, reverse cross-linking was performed at 56°C for 2 hours, followed by an overnight incubation at 80°C, and DNA was purified using isopropanol precipitation and magnetic bead separation. Following elution, 100 ng of the DNA was fragmented by sonication to 200 to 300 bp and subjected to NGS library preparation (Kapa Hyper-prep, Kapa Unique Dual indexed adapter kit (Roche, Basel, Switzerland). A total of 16 up to 20 independently prepared libraries were pooled with a total mass of 2 μg DNA, hybridized with a custom-designed capture probe panel (Table 1 and Supplemental Tables S1 and S2), washed, and amplified according to the manufacturer's instructions. The custom-designed capture

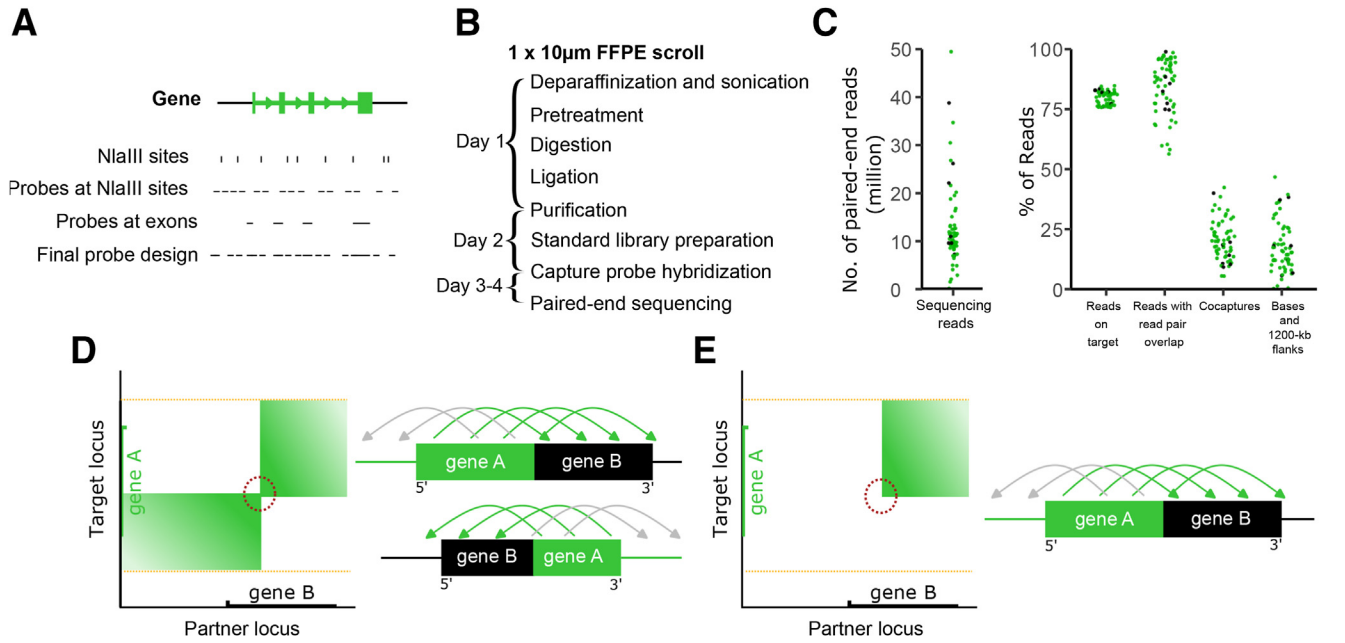

Figure 1 Evaluation of formalin-fixed, paraffin-embedded—targeted locus capture (FFPE-TLC). **A:** Schematic overview of the capture probe design. To detect rearrangements, probes are designed at all exonic regions and all NlaIII restriction sites across the entire gene, plus at least 20 kb of its flanking sequences. **B:** Overview of the FFPE-TLC workflow (related to Supplemental Figure S1). **C:** Sequencing quality control metrics of 44 FFPE tumor samples and 19 FFPE control samples. The dot plots show the number of paired-end sequencing reads, percentage of reads aligned on target, percentage of reads with read pair overlap, percentage of cocaptured reads, and percentage of bases covered in the 1200-kb flanking sequences of the targets. The decalcified FFPE samples are depicted in black, and the nondecalcified FFPE samples are depicted in green. **D** and **E:** Schematic explanation of butterfly visualizations. For each proximity-ligation—based identification of rearrangements call, the distribution of the paired-end reads with the proximity-ligated fragments (arches on top of the gene fusion event) across the genomic locus of the targeted gene (*y* axis) and the presumed rearrangement partner (*x* axis) is shown in a butterfly plot. **A** and **B:** A balanced rearrangement forms two interaction blocks, producing a butterfly appearance (**A**), whereas an unbalanced rearrangement forms a single block (**B**). The transcriptional start site of the gene is depicted with a **tick mark**. The crossover signal (highlighted in the **red dotted circle**) in the targeted locus provides information on the breakpoint location and conformation of the rearrangement. In the balanced rearrangement, the 5′ end of the target locus is separated from the 3′ end and connected to the partner locus. In the unbalanced rearrangement, only one part of a target gene fuses to a partner. A schematic representation of the formed gene fusion products is also shown. The green arches on top of the gene fusion product between the target gene and the gene fusion partner are indicative for the proximity-ligation products.

probe panel (KAPA HyperChoice; Roche) targeted 47 genes for rearrangement analysis and 2 genes for single-nucleotide variant analysis, with a total bait territory of approximately 3.3 megabases (Mb). For rearrangement analysis, probes were designed at all exonic regions and all NlaIII restriction sites across the entire gene, plus at least 20 kb of its flanking sequences (Figure 1A). Sequencing was performed on an Illumina (San Diego, CA) NovaSeq 6000 machine with 150-bp paired-end read cycles.

FFPE-TLC Data Processing

FASTQ data were aligned to the human genome build hg38 using BWA-MEM version 0.7.17-r1188 (*https://github.com/lh3/bwa*) in paired-end mode. A single paired-end read may contain multiple fragments mapping to various locations in the genome because of the proximity ligation step. Thereafter, an individual FFPE alignment file was generated for each targeted gene by demultiplexing paired-end reads that fully or partially aligned within the gene coordinate in the capture probe panel. Paired-end reads overlapping with multiple genes of the capture probe panel were assigned to multiple FFPE alignment files, and reads without any overlap were discarded.

Rearrangement Identification by PLIER

The FFPE-TLC alignment files were used for rearrangement identification by the computational pipeline PLIER, as previously described.[22] Briefly, the reference genome was first segmented *in silico* based on the recognition site of restriction enzyme NlaIII. Then, mapped fragments were overlaid on the segments. However, only one fragment was counted when more than one fragment within a read overlapped a segment. The number of segments covered by at least one fragment in equally spaced 5- and 75-kb genomic intervals was calculated, which is called proximity frequency. Proximity scores are then calculated by gaussian smoothing of proximity frequencies across each chromosome to remove local and abrupt increases (or decreases) in proximity frequencies that are most likely spurious. Next, an expected (or average) proximity score and a corresponding SD are estimated for genomic intervals with similar properties by *in silico* shuffling of observed proximity frequencies across the genome, followed by a gaussian smoothing across each chromosome. Finally, a z-score is calculated for every genomic interval using its observed proximity score and the related expected and SD of proximity scores.

Genomic intervals within 1 Mb that showed z-scores above 5.0 were merged, including the in-between intervals. For those merged intervals, the 90-percentile z-score values were calculated to get the integrated z-score. To estimate the scale-invariant enrichment score from the 5- and 75-kb interval widths, the merged intervals were grouped. The z-score value of the intervals with the largest scale (7 kb in this case) was the final enrichment score. Enrichment scores within a 3-Mb region of the targeted gene were discarded to make sure the true three-dimensional interactions between the targeted gene and its vicinity are not considered as rearrangements. In the end, a final list of calls with regions enriched in proximity-ligated products was generated for *trans* intervals with an enrichment score of $\geq$8.0, and for *cis* intervals with an enrichment score $\geq$16.0.

To assess whether PLIER-identified enrichments were true rearrangements, butterfly plots were generated for each call to present the distribution of the paired-end reads with the proximity-ligated fragments across the targeted gene and the presumed rearrangement partner. Basically, these are heat maps showing the number of captured DNA fragments that contain sequence information of both the locus of the target gene (y axis) and rearrangement partner (x axis). A balanced rearrangement forms two interaction blocks, producing a butterfly appearance; the 5′ end of the target gene preferentially forms proximity-ligation products with one side of the partner locus and is separated from the 3′ end that preferentially contacts and ligates the other part of the partner locus (5′ end of gene *A* is fused to the 3′ end of gene *B*, and 3′ end of gene *A* is fused to the 5′ end of gene *B*) (Figure 1D). On the contrary, an unbalanced rearrangement forms a single block (only one part of a target gene fuses to a partner, 5′ end of gene *A* is fused to the 3′ end of gene *B*) (Figure 1E). If no clear break or crossover signal is observed in the targeted gene, but there is random distribution of data points, then the call is considered as nonrelevant. Butterfly plots were also routinely generated for the 3-Mb region of the targeted gene that had been excluded in the PLIER assessment, to allow for detection of *cis* rearrangements by visual inspection. FFPE-TLC results were interpreted blindly, without knowledge of the results obtained by the conventional diagnostics methods to identify fusion genes.

Table 1 List of Genes in the Bone and Soft Tissue Tumor-Specific FFPE-TLC Capture Panel for Rearrangement Detection

Genes for rearrangement detection (n = 47)				
ACTB	*ERG*	*IRF2BP2*	*NUP107*	*SS18L1*
ALK	*EWSR1*	*JAZF1*	*NUTM1*	*STAT6*
ATF1	*FOS*	*KMT2A*	*NUTM2A*	*TFE3*
BCOR	*FOSB*	*MRTFB*	*PAX3*	*USP6*
BCORL1	*FOXO1*	*NAB2*	*PAX7*	*VGLL2*
BRAF	*FOXO4*	*NCOA2*	*PDGFB*	*WWTR1*
CAMTA1	*FUS*	*NR4A3*	*PHF1*	*YWHAE*
CIC	*GLI1*	*NTRK1*	*PLAG1*	
COL1A1	*HEY1*	*NTRK2*	*ROS1*	
DDIT3	*HMGA2*	*NTRK3*	*SS18*	

FFPE-TLC, formalin-fixed, paraffin-embedded—targeted locus capture.

Down-Sampling Analysis

Down-sampling analysis was automatically performed by randomly drawing reads mapping to the target of interest that underwent a rearrangement. This was done across

diluted samples and their undiluted counterparts, and each down-sampling experiment was repeated 20 times. The number of times PLIER could successfully identify the rearrangement is reported as a percentage and shown over the heat map (eg, 90% refers to 18 successful identifications of the rearrangement of 20 repeated experiments).

Fusion-Read Identification

For the fusion-read identification, split alignments (ie, individual read sequences that mapped to multiple areas in the human genome; ie, to the locus of both the target gene and the gene fusion partner) were collected. Then, the split alignments that referred to enzymatic digestion in FFPE-TLC were filtered out by discarding the split alignments that fused at the restriction enzyme recognition site (CATG). The split alignments that occurred within regions enriched in proximity-ligated products, as identified by PLIER, were collected and manually checked in a genome browser to confirm the existence of fusion reads.

Gene Fusion Detection by Conventional Diagnostic Methods

In total, 42 of 44 FFPE bone and soft tissue tumor samples had been analyzed for gene fusions in routine diagnostics by one of the five NEN-EN-ISO 15189 accredited participating centers (Supplemental Table S3). The five centers performed FISH, laboratory-developed RT-PCR, RNA sequencing, ArcherDx (custom panel/FusionPlex expanded sarcoma panel 16696 version 1.1 (ArcherDx, Inc., Boulder, CO) (Supplemental Table S2), and/or custom-designed NanoString nCounter FusionPlex (NanoString Technologies, Inc., Seattle, WA), according to their usual protocols (University Medical Center Groningen Laboratory for Molecular Pathology, *http://www.moloncopath.nl*, last accessed April 1, 2022).[7,16,23]

Data Availability

The raw sequencing data in this article are available from the corresponding author on reasonable request as restrictions apply to the availability of these patient data.

Results

Processing of Bone and Soft Tissue Tumor Samples with FFPE-TLC

A bone and soft tissue tumor-specific FFPE-TLC capture panel was designed, which differed from the lymphoma-specific panel[22] in terms of both number of targeted genes and bait design. The bone and soft tissue tumor-specific panel targets a total of 47 genes for rearrangement analysis (Table 1). A spaced bait design based on NlaIII restriction sites present across the entire gene rather than a tiled design was followed (Figure 1A) to selectively pull down proximity-ligated products that formed after NlaIII digestion. This smoothens the NGS coverage and reduces the number of reads needed while not compromising rearrangement detection. The number of genes targeted by FFPE-TLC is comparable to other NGS-based methods for bone and soft tissue tumor classification (ie, ArcherDx FusionPlex expanded sarcoma panel) (Supplemental Table S2).

A set of 44 FFPE tumor samples, encompassing 26 different types of bone and soft tissue tumors, and 19 FFPE control samples was subjected to FFPE-TLC library preparation (Figure 1B). FFPE-TLC only requires 3 to 4 days from sample preparation to sequence data (Figure 1B). Seven FFPE samples were decalcified following procedures with picric acid, formic acid, or EDTA solutions during diagnostic preparations in the clinical centers. All samples passed the authors' standard and FFPE-TLC–specific NGS quality control metrics (ie, percentage of aligned reads, percentage of reads on target, and percentage of reads with proximity-ligated fragments). No apparent differences in quality control metrics were noted between decalcified and nondecalcified FFPE samples (Figure 1C and Supplemental Table S3).

Identification of Rearrangements

PLIER, a computational pipeline for the analysis of FFPE-TLC sequencing data,[22] was used to identify genomic intervals with significant accumulation of proximity-ligation events formed with a given target gene: such chromosomal sites are candidate rearrangement partners of this gene of interest. Subsequently, as previously described,[22] butterfly plots were generated that present the distribution of these proximity-ligation events between the targeted gene and presumed rearrangement partner. Inspection of butterfly plots allows finding the chromosomal breakpoint locations, needed to unambiguously determine whether a candidate rearrangement truly involves the target gene of interest and whether the rearrangement is balanced or unbalanced (Figure 1D).[22] A total of 58 rearrangements were identified by FFPE-TLC in 40 of 44 FFPE tumor samples, whereas none was found in any of the FFPE control samples (Table 2 and Supplemental Table S3). For 31 of 58 rearrangements, the actual fusion read (or breakpoint sequence) was also found, confirming the PLIER-identified rearrangement at bp level (Supplemental Table S4).

Rearrangements Resulting in Gene Fusions

Most rearrangements identified by FFPE-TLC were well-known gene fusions for bone and soft tissue tumors (Figure 2A, Table 1, and Supplemental Figures S2–S5). For instance, *SS18*::*SSX1* and *SS18*::*SSX2* gene fusions were identified in five synovial sarcomas, *FUS*::*DDIT3* was identified in three myxoid liposarcomas, and *EWSR*-related fusions were identified in three clear cell sarcomas. An

Table 2 FFPE-TLC—Identified Rearrangements Compared with Conventional Test Results

ID	Tumor type	Consensus fusion gene	FFPE-TLC fusion gene and other rearrangements	FISH rearrangement	Archer/RT-PCR/ RNA-seq fusion gene	NanoString fusion gene	Discordance
F335	Synovial sarcoma	*SS18* (chr18) rearrangement	*SS18*-chrX: 108 Mb (intergenic), *SS18*-chr18: 9 Mb (*ANKRD12*), *SS18*-chr18: 0.5 Mb (intergenic)	*SS18*	NA	*SS18* imbalance	No
F336	Synovial sarcoma	*SS18* (chr18)::*SSX1* (chrX)	*SS18::SSX1*, *SS18*-chr3: 50 Mb (*CACNA2D2*)	*SS18*	NA	*SS18::SSX1*	No
F337	Ewing sarcoma	*EWSR1* (chr22)::*FLI1* (chr11)	*EWSR1::FLI1*, *EWSR1*-chr11: 92 Mb (intergenic), *EWSR1*-chr11: 114 Mb (intergenic)	*EWSR1*	NA	*EWSR1::FLI1*	No
F428	Myxoid liposarcoma	*FUS* (chr16)::*DDIT3* (chr12)	*FUS::DDIT3*	*DDIT3*	NA	*FUS::DDIT3*	No
F431	Ewing sarcoma	*EWSR1* (chr22)::*FLI1* (chr11)	*EWSR1::FLI1*	*EWSR1::FLI1*	NA	*EWSR1::FLI1*	No
F338	Ewing sarcoma	*EWSR1* (chr22)::*ERG* (chr21)	*EWSR1::ERG*, *ERG*-chr3: 124 Mb (*KALRN*)	***EWSR1* (below cutoff)**	NA	*EWSR1::ERG*	**Yes**
F434	Low-grade endometrial stroma sarcoma	*JAZF1* (chr7) rearrangement	*JAZF1::SUZ12*, *JAZF1*-chr8: 22 Mb (*BMP1*)	*JAZF1*	NA	**None***	**Yes**
F437	Biphasic synovial sarcoma	*SS18* (chr18) rearrangement	*SS18::SSX1*, *SS18*-chr2: 125 Mb (intergenic)	*SS18*	NA	***SS18::SSX4***	**Yes**
F583	Synovial sarcoma	*SS18* (chr18) rearrangement	*SS18::SSX2*	*SS18*	***SS18::SSX4***	NA	**Yes**
F427	Clear cell (sinonasal) sarcoma	*EWSR1* (chr22)::*COLCA2* (chr11)	*EWSR1::COLCA2*	*EWSR1*	*EWSR1::COLCA2*	None†	No
F433	Inflammatory myofibroblastic tumor	*THBS1* (chr15)::*ALK* (chr2)	*THBS1::ALK*	*USP6* (negative)	*THBS1::ALK*	NA	No
F588	Aneurysmal bone cyst	*USP6* (chr17) rearrangement	*CDH11::USP6*	*USP6*	**Did not pass QC**	NA	No
F388	Synovial sarcoma	*SS18* (chr18) rearrangement	*SS18::SSX1*	*SS18*	NA	NA	No
F389	Clear cell sarcoma	*EWSR1* (chr22) rearrangement	*EWSR1::ATF1*	*EWSR1*	NA	NA	No
F390	Well-differentiated liposarcoma	Negative	Amp on chr12 (including *MDM2*)	*MDM2/CEP12*	NA	NA	No
F391	Myxoid liposarcoma	*DDIT3* (chr12) rearrangement	*FUS::DDIT3*	*DDIT3*	NA	NA	No
F394	Alveolar rhabdomyosarcoma	*FOXO1* (chr13) rearrangement	*PAX7::FOXO1*, amp on chr2 (including *MYCN*)	*FOXO1*	NA	NA	No
F395	Dermatofibrosarcoma protuberans	*COL1A1* (chr17) rearrangement	*COL1A1::PDGFB*	*COL1A1*	NA	NA	No
F397	Low-grade fibromyxoid sarcoma	*FUS* (chr16) rearrangement	*FUS::CREB3L1*, chr1: 117 (intergenic)—*FUS*	*FUS*	NA	NA	No
F398	Synovial sarcoma	*SS18* (chr18) rearrangement	*SS18::SSX2*, amp on chr4 (including *PDGFRA*)	*SS18*	NA	NA	No

(*table continues*)

Table 2 (*continued*)

ID	Tumor type	Consensus fusion gene	FFPE-TLC fusion gene and other rearrangements	FISH rearrangement	Archer/RT-PCR/ RNA-seq fusion gene	NanoString fusion gene	Discordance
F432	Nodular fasciitis	*USP6* (chr17) rearrangement	*MIR22HG::USP6*	*USP6* (borderline)	NA	NA	No
F435	Myoepithelioma	*EWSR1* (chr22) rearrangement	*EWSR1::PBX3*	*EWSR1*	NA	NA	No
F436	Malignant lesion	Negative	Negative	*EWSR1* and *FUS* (negative)	NA	NA	No
F339	Ewing sarcoma	*EWSR1* (chr22)::*ERG* (chr21)	*EWSR1::ERG*, *GAS2L1* (downstream of *EWSR1*)—chr8: 102 Mb (intergenic)	NA	*EWSR1::ERG*	*EWSR1::ERG*	No
F582	Infantile fibrosarcoma	*ETV6* (chr12)::*NTRK3* (chr15)	*ETV6::NTRK3*	NA	*ETV6::NTRK3*	*ETV6::NTRK3*	No
F342	Cellular myxoma	Negative	Negative	NA	*FUS::CREB2L2* negative	NA	No
F344	Low-grade osteosarcoma	Negative	Amp on chr12 (including *MDM2*)	NA	*HEY1::NCOA2* negative	NA	No
F392	Atypical spindle cell/ pleomorphic lipomatous tumor	*HMGA2* (chr12)::*CDK14* (chr7)	*HMGA2::CDK14*, *RPSAP52* (upstream of *HMGA2*)—chr12: 28 Mb (XR_931461.2)	NA	*HMGA2::CDK14*‡	NA	No
F426	Myoepithelioma	Negative	*CAMTA1*::intergenic	NA	Negative	NA	No
F573	Extraskeletal myxoid chondrosarcoma	*EWSR1* (chr22)::*NR4A3* (chr9)	*EWSR1::NR4A3*	NA	*EWSR1::NR4A3*	NA	No
F581	Mesenchymal chondrosarcoma	*HEY1* (chr8)::*NCOA2* (chr8)	*HEY1::NCOA2*, *HEY1*-chr8: 118 Mb (intergenic)	NA	*HEY1::NCOA2*	NA	No
F584	Extraskeletal myxoid chondrosarcoma	*TAF15* (chr17)::*NR4A3* (chr9)	*TAF15::NR4A3*	NA	*TAF15::NR4A3*	NA	No
F585	Aneurysmal bone cyst	*CDH11* (chr16)::*USP6* (chr17)	*CDH11::USP6*	NA	*CDH11:: USP6*§	NA	No
F586	Clear cell sarcoma	*EWSR1* (chr22)::*CREB1* (chr2)	*EWSR1::CREB1*, chr8: 58 Mb (*SDCBP*) —*EWSR1*, amp on chr8	NA	*EWSR1::CREB1*	NA	No
F587	Aneurysmal bone cyst	*PAFAH1B1* (chr17)::*USP6* (chr17)¶	*PAFAH1B1::USP6*¶	NA	*PAFAH1B1::USP6*	NA	No
F589	Myoepithelioma	*FUS* (chr16)::*POU5F1* (chr6)	*FUS::POU5F1*, chr16: 18 Mb (intergenic)—*FUS*	NA	*FUS::POU5F1*	NA	No
F590	Ossifying fibromyxoid tumor	*MEAF6* (chr1)::*PHF1* (chr6)	*MEAF6::PHF1*	NA	*MEAF6::PHF1*	NA	No
F572	Ewing sarcoma	*EWSR1* (chr22)::*FLI1* (chr11)	*EWSR1::FLI1*	NA	NA	*EWSR1::FLI1*	No
F574	Epithelioid hemangioendothelioma	*WWTR1* (chr3)::*CAMTA1* (chr1)	*WWTR1::CAMTA1*	NA	NA	*WWTR1::CAMTA1*	No
F576	Myxoid liposarcoma	*FUS* (chr16)::*DDIT3* (chr12)	*FUS::DDIT3*	NA	NA	*FUS::DDIT3*	No

(*table continues*)

Table 2 (*continued*)

ID	Tumor type	Consensus fusion gene	FFPE-TLC fusion gene and other rearrangements	FISH rearrangement	Archer/RT-PCR/ RNA-seq fusion gene	NanoString fusion gene	Discordance
F579	Dermatofibrosarcoma protuberans with fibrosarcomatous progression (grade 3)	*COL1A1* (chr17)::*PDGFB* (chr22)	*COL1A1::PDGFB*, amp on chr12	NA	NA	*COL1A1::PDGFB*	No
F575	Epithelioid hemangio-endothelioma	*WWTR1* (chr3)::*CAMTA1* (chr1)	*WWTR1::CAMTA1*	NA	NA	**None**‖	**Yes**
F340	Giant cell tumor of bone	Negative	Negative	NA	NA	NA	No
F341	Giant cell tumor of bone	Negative	Negative	NA	NA	NA	No

Discrepant results between FFPE-TLC and the conventional test results are highlighted in bold.
*NanoString identified also other gene fusions with high counts; therefore, *JAZF1* fusion not reported.
†*EWSR1::COLCA2* not present in NanoString panel.
‡ArcherDx initially not performed in diagnostics.
§Analysis performed on fresh-frozen tissue.
¶FFPE-TLC initially missed this in *cis* call.
‖*WWTR1::CAMTA1* not identified by NanoString; no FFPE material left for re-analysis.
Amp, amplification; chr, chromosome; FFPE-TLC, formalin-fixed, paraffin-embedded—targeted locus capture; FISH, fluorescence *in situ* hybridization; ID, identifier; Mb, megabases; NA, not analyzed; QC, quality control; RNA-seq, RNA sequencing.

EWSR1::COLCA2 gene fusion, a rare but recurrent fusion in a specific subtype,[24] was observed in the sinonasal sarcoma. In addition, a novel gene fusion, *HMGA2::CDK14*, was detected in an atypical spindle cell/pleomorphic lipomatous tumor (sample F392) (Figure 2B).[1,25] The butterfly plot of this gene fusion showed an unbalanced rearrangement in which the 5′ end of *HMGA2* is fused to the 3′ end of *CDK14* (Figure 2, C and D). The actual genomic breakpoint was found in intron 4 of *HMGA2* (NM_003483) and intron 13 of *CDK14* (NM_012395) (NM_numbers are searchable in Ensembl, *https://www.ensembl.org*, last accessed November 1, 2022). This was predicted, and later confirmed, on RNA level with the ArcherDx FusionPlex Expanded Sarcoma assay, to result in an in-frame fusion transcript leading to truncation of *HMGA2*. At time of diagnosis, there were no histopathologic indications for gene fusion analysis (Figure 2B and Supplemental Figure S6). The butterfly plot also showed lack of proximity-ligation products of *HMGA2* with its naturally upstream sequences. In fact, chromosome 12p11.22 sequences are upstream of the *HMGA2::CDK14* gene fusion (Supplemental Tables S3 and S4). This additional rearrangement, which occurred intrachromosomally, remained undetected by ArcherDx.

Butterfly visualization of all these well-known gene fusions showed their involvement in balanced and unbalanced rearrangements (Supplemental Figures S2–S5). An example of a reciprocal but complex rearrangement observed in the alveolar rhabdomyosarcoma sample (sample F394) (Supplemental Figure S6) is provided in Figure 2, E and F. The *FOXO1::PAX7* gene fusion that combines the 5′ end (start) of *FOXO1* (chromosome 13) with the 3′ end (end) of *PAX7* (chromosome 1) is clearly still part of chromosome 13, because the 3′ end of *PAX7* not only forms ligation products with the 5′ end of *FOXO1*, but also with its upstream sequences on chromosome 13. In contrast, the reciprocal and oncogenic *PAX7::FOXO1* gene fusion appears not part of chromosome 13 or 1 sequences, as the 5′ end of *PAX7* and the 3′ end of *FOXO1* exclusively form ligation products with each other, not with their naturally flanking sequences. This suggests that the *PAX7::FOXO1* gene fusion exists on extrachromosomal DNA. Moreover, the extremely high number of ligation products suggests that this extrachromosomal DNA is highly amplified. The identified genomic breakpoint sequences within the *PAX7* and *FOXO1* locus enabled reconstructing the configuration of the extrachromosomal circular DNA (Figure 2, G and H, and Supplemental Table S4). Another striking observation was detected in a low-grade endometrial stromal sarcoma, which presented with a double (bi-allelic) *JAZF1* fusion (sample F434). Balanced rearrangements were observed with the fusion partners *SUZ12* and *BMP1*; however, only the *JAZF1::SUZ12* was predicted to result in an in-frame fusion transcript. The *JAZF1* and *BMP1* fusion presented with an incorrect orientation of the genes. The butterfly visualization showed that the 5′ ends of *JAZF1* and *BMP1* and 3′ ends of *JAZF1* and *BMP1* were fused, which will not result in a functional fusion transcript (Supplemental Figures S2–S5). These examples illustrate that FFPE-TLC not only identifies the gene fusion, but also provides details on the complexity of the event.

Other Rearrangements

Rearrangements not leading to a gene fusion were also observed in several FFPE tumor samples (Table 2 and Supplemental Table S3). These included rearrangements with one genomic breakpoint localized in an intergenic region, chromosomal amplifications, and more complex rearrangements. One of the gene::intergenic fusions was found in a myoepithelioma (sample F426) (Figure 2I and Supplemental Figure S6) that presented with P40 [an isoform of p63 (deltaNp63)] and diffuse cytokeratin-7 (CK-7) and S-100 positivity. The butterfly plot uncovered that the 5′ end of *CAMTA1* was fused to an intergenic region upstream of *KHDRBS1* (Figure 2, J and K). However, the genomic breakpoint sequence implied that the 3′ end of *CAMTA1* was involved. Subsequent intragenic analysis for breakpoint sequences revealed a small deletion and inversion in intron 5 of *CAMTA1* (NM_015215, searchable in Ensembl, *https://www.ensembl.org*, last accessed November 1, 2022), which supports the findings of the butterfly visualization. Chromosomal amplifications were detected as several targeted genes showed significant enrichment of proximity-ligated products in the same region. Some of these amplifications are known driver molecular alterations [eg, an amplified region on chromosome 12 containing several genes, including *MDM2*, was observed in a low-grade osteosarcoma and well-differentiated liposarcoma (samples F344 and F390) and an amplified region on chromosome 2 containing *MYCN* was observed in an alveolar rhabdomyosarcoma (sample F394)]. Complex rearrangements were seen in a synovial sarcoma, which harbored several *SS18* rearrangements with intrachromosomal and interchromosomal partners (Supplemental Figures S2–S5).

FFPE-TLC versus Conventional Diagnostic Methods

To compare the detection of rearrangements by FFPE-TLC with conventional diagnostic methods, results of 43 samples that underwent prior rearrangement analysis with one or more conventional diagnostic methods were retrieved from

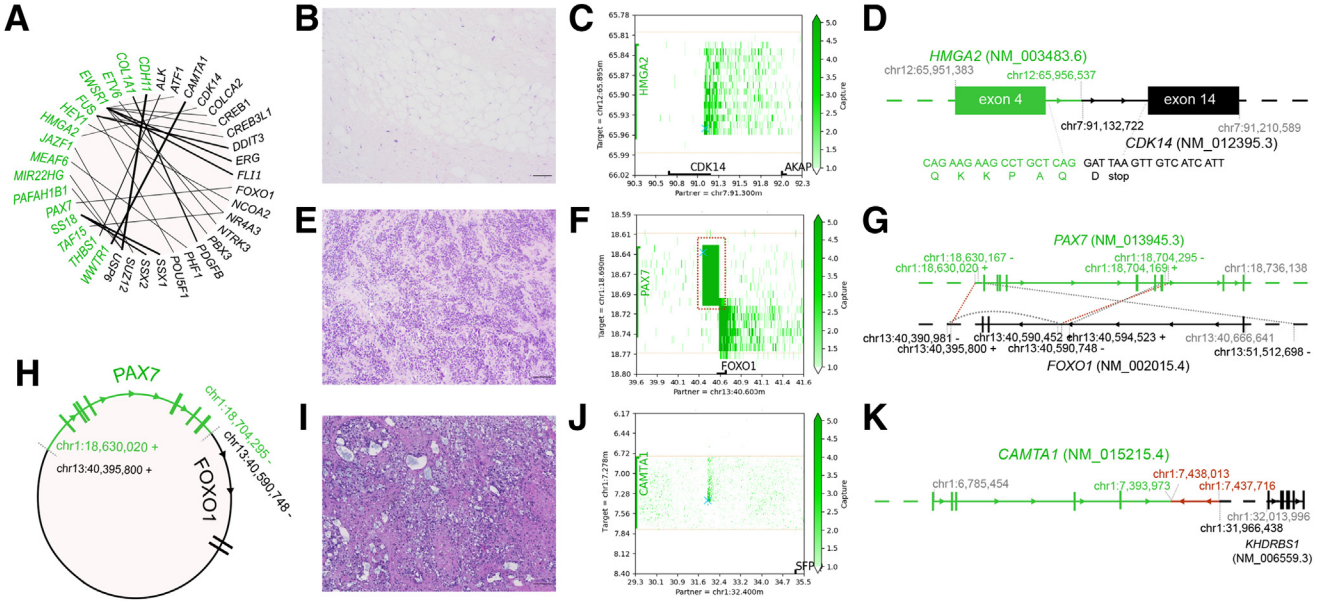

Figure 2 Rearrangements resulting in gene fusions. **A:** Circos plot showing an overview of all identified rearrangements resulting in gene fusions in the 44 formalin-fixed, paraffin-embedded tumor samples. The 5′- and 3′-end partners of the gene fusion are depicted in black and green, respectively. **B:** Representative image from hematoxylin and eosin (H&E) staining of the atypical spindle cell/pleomorphic lipomatous tumor (sample F392) showing atypical spindle cells irregularly admixed with adipocytic cells. The atypical spindle tumor cells show an ill-defined, pale eosinophilic cytoplasm with hyperchromatic nuclei, set in a collagenous stroma. Bizarre, hyperchromatic, and pleomorphic multinucleated cells are scattered within the spindle cells and adipocytes. **C:** Butterfly visualization of the novel *HMGA2*::*CDK14* gene fusion that was identified in an atypical spindle cell/pleomorphic lipomatous tumor (sample F392). A total of 1301 paired-end reads with proximity-ligated products show that the 5′ end of *HMGA2* is fused to the 3′ end of *CDK14*. **D:** Schematic representation of the *HMGA2*::*CDK14* gene fusion and predicted fusion transcript leading to truncation of *HMGA2*. Not to scale. **E:** Representative image from H&E staining of the alveolar rhabdomyosarcoma (sample F394). **F:** Butterfly visualization of a *PAX7*::*FOXO1* gene fusion. The reciprocal fusion of the 5′ end of *PAX7* to the 3′ end of *FOXO1*, indicated in the **red boxed area**, lacks proximity-ligated products in the flanking sequences (upstream of *PAX7* and downstream of *FOXO1*). This suggests that the *PAX7*::*FOXO1* gene fusion exists on extrachromosomal DNA. **G:** Breakpoint locations within the *PAX7* and *FOXO1* locus for the *PAX7*::*FOXO1* gene fusion. The orientation of the breakpoint junctions is indicated with a + (5′ end of fragment) or − (3′ end of fragment). The breakpoint junctions on extrachromosomal DNA are indicated with **red dotted lines**. Not to scale. **H:** Predicted visualization of *PAX7*::*FOXO1* gene fusion on extrachromosomal circular DNA. Not to scale. **I:** Representative image from H&E staining of the myoepithelioma (sample F426) showing tumor cells with eosinophilic cytoplasm and prominent nucleoli and few areas of squamous-like metaplasia with focal dyskeratosis. **J** and **K:** Butterfly visualization and schematic overview of *CAMTA1* intergenic rearrangement. Scale bars = 100 μm (**B**, **E**, and **I**). Chr, chromosome; m, megabase.

the five participating centers. The five centers used a wide range of conventional diagnostic methods, including FISH, RT-PCR, RNA sequencing, ArcherDx (custom panel/FusionPlex expanded sarcoma panel), and custom-designed NanoString nCounter FusionPlex. Although most samples were analyzed with a single method, 14 samples were diagnosed with two methods. The overall success rate of the conventional diagnostic methods was 98%; only one sample failed RNA quality control in the ArcherDx.

FFPE-TLC results were highly concordant with the conventional diagnostic methods (Tables 2 and 3). Small discrepancies were observed in five samples. In two synovial sarcomas, FFPE-TLC identified *SS18::SSX1* and *SS18::SSX2* gene fusions, whereas ArcherDx and NanoString identified *SSX4* as fusion partner (samples F437 and F583). The *SSX* genes are highly homologous[5,7,26] and, therefore, difficult to distinguish on breakpoint sequence alone. FFPE-TLC with PLIER analysis can easily identify the correct gene fusion partner (Supplemental Figure S7), as the proximity-ligation step generates broad sequencing coverage across the fusion partner. In the low-grade endometrial stromal sarcoma with a double *JAZF1* fusion, a double fusion signal was also observed with *JAZF1* break-apart FISH. As expected, only the in-frame fusion gene (*JAZF1::SUZ12*) leading to an expressed transcript was uncovered with ArcherDx; however, the gene fusion(s) remained below detection limit by NanoString (sample F434). NanoString also failed to detect a gene fusion in sample F575, and FFPE-TLC identified a *WWTR::CAMTA1* gene fusion that was predicted to produce an in-frame fusion transcript. Unfortunately, insufficient FFPE material was left for re-analysis or independent confirmation. The other discrepancy was observed because split signals were below the FISH positivity threshold of 30% for *EWSR1* (sample F338). Overall, FFPE-TLC with PLIER analysis achieved a high specificity (no false positives) and sensitivity (no false negative) for the detection of fusion genes.

Limit of Detection for Rearrangement Identification by FFPE-TLC

The aim of this study was to determine whether FFPE-TLC and PLIER analysis can easily be applied to additional tumor types, with different samples and different panel designs. Following the successful identification of rearrangements, the limit of detection was determined using contrived admixtures of gene fusion-negative and gene fusion-positive FFPE samples. The five gene fusions with a 5% variant allele frequency were detected in all replicates, even when the total number of sequencing reads across the whole panel was sampled to 5 million paired-end reads (Table 4). When down sampling to 2.5 million paired-end reads, PLIER still identified the gene fusion in 98% of the replicates. For all (undiluted) samples in this study, the total number of paired-end reads ranged from 0.12 to 49.49 million reads (median, 10.68 million reads) (Supplemental Table S3). At least 5 million paired-end reads were also obtained for the five rearrangement-negative tumor samples and 19 control samples. An *EWSR1::FLI1* gene fusion was identified with merely 117,243 paired-end reads in an Ewing sarcoma sample, but this sample, according to FISH, contained a high tumor load.

Discussion

This study investigated the applicability of the DNA-based FFPE-TLC technology for rearrangement detection in bone and soft tissue tumor samples and compared the results with conventional diagnostic methods. FFPE-TLC was successfully applied to all decalcified and nondecalcified FFPE samples from the five participating centers. Straightforwardly, rearrangements resulting in either gene fusions or other chromosomal changes were identified in 40 of 44 FFPE tumor samples. Comparison with conventional methods revealed five discordant cases, in which FFPE-TLC could identify gene fusions, and other methods had failed mainly because of detection limits. The high concordance to conventional diagnostic methods and a limit of detection of 5% variant allele frequency denote the potential of FFPE-TLC as a reliable alternative for routine molecular diagnostics.

With FFPE-TLC, novel and known rearrangements can be successfully identified independent of cancer type, breakpoint sequence, and complexity of the genomic event.[22] In one sample, FFPE-TLC revealed a novel fusion partner for *HMGA2*, which expands the genetic spectrum of bone and soft tissue tumors. *HMGA2* is often rearranged in lipomas; however, the functional and clinical significance of *HMGA2::CDK14* remains untested. This particular sample also presented with an *RB1* deletion; therefore, ArcherDx gene fusion analysis was initially not performed for molecular diagnostics. Similarly, the clinical significance remains unknown for the unique observation in the alveolar rhabdomyosarcoma sample, which contained the amplified *PAX7::FOXO1* gene fusion on extrachromosomal DNA. There is evidence that gene fusion status is essential for prognostic stratification of patients with alveolar rhabdomyosarcoma.[27] However, despite *PAX3* and *PAX7::FOXO1* gene fusions having been previously identified to be amplified on extrachromosomal elements,[28] the presence and amplification on extrachromosomal DNA have not been taken into account as factors in these prognostic studies. The additional information provided by FFPE-TLC, beyond the driver gene of the gene fusion, may be an important determinant for diagnosis, prognosis, and treatment.

When compared with conventional diagnostic methods, FFPE-TLC showed high performance in detecting gene fusions. More important, FFPE-TLC could identify gene fusions where conventional methods had failed due to either detection limits (FISH and NanoString) or poor sample quality (ArcherDx). The poor sample quality may be the

Table 3 FFPE-TLC versus Conventional Diagnostic Methods

	FISH			ArcherDx/ RNA-seq/ RT-PCR			NanoString			Combined		
Method	No	Yes	NA	No	Yes	NA	No	Yes	NA	No	Yes	NA
PLIER												
No	1	0	3	2	0	6	0	0	7	3	0	16
Yes	**1***	20	19	**1**†	13	22	**2**‡	13	22	**4**	45	64

The discrepant results are highlighted in bold.
*Sample F338.
†Sample F588.
‡Samples F434 and F575.
FFPE-TLC, formalin-fixed, paraffin-embedded—targeted locus capture; FISH, fluorescence *in situ* hybridization; NA, not analyzed; PLIER, proximity-ligation—based identification of rearrangements; RNA-seq, RNA sequencing.

result of decalcification.[29] Previous studies have also reported a higher failure rate for gene fusion detection in decalcified FFPE samples using an RNA-based assay.[7,30] The use of milder decalcifying agents, such as EDTA, has been advocated as they have been shown to yield better RNA/DNA quality from decalcified FFPE tissue. In this study, no apparent differences in quality control metrics were noted between the acid-decalcified and EDTA-decalcified and nondecalcified FFPE samples, but only a few decalcified samples were analyzed. The (potentially) enhanced gene fusion detection of FFPE-TLC in decalcified samples requires expanded analysis with comparison to the conventional diagnostic methods.

Besides the high performance, FFPE-TLC offers additional significant benefits over the conventional methods, FISH, ArcherDx, and/or NanoString. First, FFPE-TLC requires only a single FFPE slide (10 μm thick) as starting material to simultaneously analyze multiple targets. Second, after the initial proximity-ligation steps, FFPE-TLC follows the standard DNA-based targeted NGS workflow, which allows researchers to simultaneously assess other genetic variations (eg, single-nucleotide variations, copy number variations, and microsatellite instability). Such an all-in-one workflow, which only requires 1 extra day compared with the current DNA-based NGS tests, will positively impact the turnaround time and labor costs. Third, FFPE-TLC can detect gene fusion partners without prior knowledge following a relatively simple bioinformatic workflow. However, some potential gene fusion partners (like *SSX* genes[5,7,26]) exhibit significant homology between each other. Collectively, FFPE-TLC could become a diagnostic alternative to the conventional diagnostic methods.

One challenge of the conventional DNA-based targeted NGS is to detect gene fusions in intronic regions, because introns cannot always be fully covered by capture probes because of either repetitive regions or the large intron size, resulting in a lower sensitivity. FFPE-TLC is also based on regular capture protocols but can overcome these challenges as the proximity-ligation step generates broad sequencing coverage and allows for gene fusion detection independent of the identification of the breakpoint fusion read. Following specific capture design rules, many (large) genes can simultaneously be analyzed for their involvement in rearrangements. On updates in the molecular testing guidelines, FFPE-TLC, like other capture-based NGS technologies, can easily expand the gene panel. In this study, the exceptionally large introns of *NTRK1-3* with numerous repetitive elements were also covered without impairing sequencing efficiency. Despite the spaced probing, breakpoint sequences were still identified in most of the gene fusion-positive FFPE samples. These DNA breakpoint sequences could serve as potential biomarkers to monitor disease progression.

Although FFPE-TLC offers several advantages over the conventional methods, the bioinformatic workflow that worked well on lymphomas and bone and soft tissue tumors can be further optimized to be more effective in routine

Table 4 Limit of Detection for Rearrangement Identification by FFPE-TLC with PLIER Analysis

			Repeats = 20											
			10 M			7.5 M			5 M			2.5 M		
Sample	Target	Partner	5%	2%	0.50%	5%	2%	0.50%	5%	2%	0.50%	5%	2%	0.50%
F429	*ALK*	*CLTC*	NA	NA	NA	100	NA	NA	100	100	0	100	100	0
F391	*FUS*	*DDIT3*	100	100	100	100	100	100	100	100	100	100	100	100
F391	*DDIT3*	*FUS*	100	100	100	100	100	100	100	100	100	100	100	100
F339	*ERG*	*EWSR1*	100	90	15	100	80	15	100	15	25	100	25	5
F339	*EWSR1*	*ERG*	100	0	0	100	0	0	100	0	10	90	0	10
F388	*SS18*	*SSX1*	100	100	100	100	100	100	100	100	100	100	100	90
F336	*SS18*	*SSX1*	100	100	0	100	100	0	100	100	0	100	90	0

The number of times PLIER could successfully identify the rearrangement is reported as a percentage (eg, 90% refers to 18 successful identifications of the rearrangement of 20 repeated experiments).
FFPE-TLC, formalin-fixed, paraffin-embedded—targeted locus capture; M, million reads; NA, not analyzed; PLIER, proximity-ligation—based identification of rearrangements.

diagnostics. Currently, the butterfly visualizations of the PLIER-identified enrichments are manually inspected for true rearrangements. This requires a short training session and minimum effort. The number of PLIER-identified enrichments per sample is low, especially when a known list of background regions (ie, centromeric and telomeric regions) is generated, which also have high enrichment scores in control samples. In addition, the 3-Mb region surrounding each target is visualized in butterfly plots to manually identify in *cis* rearrangements. Hence, the workflow can benefit from automated interpretation of the butterfly plots. However, additional studies with samples containing in *cis* rearrangements need to be performed to develop such an interpreter in the current workflow.

The several conventional methods used by the five participating centers illustrate the lack of standardization for fusion gene detection in bone and soft tissue tumors. Together with the emerging understanding that distinct gene fusions result in different entities of bone and soft tissue tumors with distinct prognostic and therapeutic implications,[5] reliable and robust detection of these gene fusions is essential. FFPE-TLC has the potential to become a good alternative assay because of its sensitivity, good performance, and lack of pre-existing sequence knowledge. And, above all, it's a DNA-based NGS technology, allowing a single workflow in routine diagnostics.

Acknowledgment

We thank Cheryl Dambrot for editing this manuscript.

Author Contributions

W.d.L., H.F., and E.Sp. conceived, initiated, and supervised the project; R.W.J.M., W.W.J.d.L., A.-M.C.-J., J.V.M.G.B., L.C.v.K., J.V.d.M., D.C., and S.v.H. selected samples and collected data; J.F.S. performed all formalin-fixed, paraffin-embedded–targeted locus capture experiments; E.St., A.A., K.H., and M.C. processed sequencing data; J.F.S., E.St., R.W.J.M., A.A., A.-M.C.-J., J.V.M.G.B., L.C.v.K., J.V.d.M., D.C., S.v.H., W.d.L., H.F., and E.Sp. analyzed data; R.W.J.M. and E.St. prepared figures and tables and wrote the manuscript; all authors edited and approved the manuscript.

Supplemental Data

Supplemental material for this article can be found at *http://doi.org/10.1016/j.jmoldx.2023.06.012*.

References

1. WHO Classification of Tumours Editorial Board: Soft Tissue and Bone Tumours. WHO Classification of Tumours, 5th Edition, Volume 3. Lyon, France, International Agency for Research on Cancer, 2020
2. Mertens F, Antonescu CR, Mitelman F: Gene fusions in soft tissue tumors: recurrent and overlapping pathogenetic themes. Genes Chromosomes Cancer 2016, 55:291–310
3. Abeshouse A, Adebamowo C, Adebamowo SN, Akbani R, Akeredolu T, Ally A, et al: Comprehensive and integrated genomic characterization of adult soft tissue sarcomas. Cell 2017, 171: 950–965.e28
4. Nacev BA, Sanchez-Vega F, Smith SA, Antonescu CR, Rosenbaum E, Shi H, et al: Clinical sequencing of soft tissue and bone sarcomas delineates diverse genomic landscapes and potential therapeutic targets. Nat Commun 2022, 13:3405
5. Gounder MM, Agaram NP, Trabucco SE, Robinson V, Ferraro RA, Millis SZ, et al: Clinical genomic profiling in the management of patients with soft tissue and bone sarcoma. Nat Commun 2022, 13:3406
6. Bishop R: Applications of fluorescence in situ hybridization (FISH) in detecting genetic aberrations of medical significance. Bioscience Horizons 2010, 3:85–95
7. Lam SW, Cleton-Jansen A-M, Cleven AHG, Ruano D, van Wezel T, Szuhai K, Bovée JVMG: Molecular analysis of gene fusions in bone and soft tissue tumors by anchored multiplex PCR–based targeted next-generation sequencing. J Mol Diagn 2018, 20:653–663
8. Tachon G, Cortes U, Richard S, Martin S, Milin S, Evrard C, Lamour C, Karayan-Tapon L: Targeted RNA-sequencing assays: a step forward compared to FISH and IHC techniques? Cancer Med 2019, 8:7556–7566
9. Lanic M-D, le Loarer F, Rainville V, Sater V, Viennot M, Beaussire L, Viailly P-J, Angot E, Hostein I, Jardin F, Ruminy P, Laé M: Detection of sarcoma fusions by a next-generation sequencing based–ligation-dependent multiplex RT-PCR assay. Mod Pathol 2022, 35:649–663
10. Zhu G, Benayed R, Ho C, Mullaney K, Sukhadia P, Rios K, Berry R, Rubin BP, Nafa K, Wang L, Klimstra DS, Ladanyi M, Hameed MR: Diagnosis of known sarcoma fusions and novel fusion partners by targeted RNA sequencing with identification of a recurrent ACTB-FOSB fusion in pseudomyogenic hemangioendothelioma. Mod Pathol 2019, 32:609–620
11. Papp G, Mihály D, Sápi Z: Unusual signal patterns of break-apart FISH probes used in the diagnosis of soft tissue sarcomas. Pathol Oncol Res 2017, 23:863–871
12. Carithers LJ, Agarwal R, Guan P, Odeh H, Sachs MC, Engel KB, Greytak SR, Barcus M, Soria C, Lih CJ, Williams PM, Branton PA, Sobin L, Fombonne B, Bocklage T, Andry C, Duffy ER, Sica G, Dhir R, Jewell S, Roche N, Moore HM: The biospecimen preanalytical variables program: a multiassay comparison of effects of delay to fixation and fixation duration on nucleic acid quality. Arch Pathol Lab Med 2019, 143:1106–1118
13. Chang KTE, Goytain A, Tucker T, Karsan A, Lee C-H, Nielsen TO, Ng TL: Development and evaluation of a pan-sarcoma fusion gene detection assay using the NanoString nCounter platform. J Mol Diagn 2018, 20:63–77
14. Patel NR, Chrisinger JSA, Demicco EG, Sarabia SF, Reuther J, Kumar E, Oliveira AM, Billings SD, Bovée JVMG, Roy A, Lazar AJ, Lopez-Terrada DH, Wang W-L: USP6 activation in nodular fasciitis by promoter-swapping gene fusions. Mod Pathol 2017, 30:1577–1588
15. Heyer EE, Deveson IW, Wooi D, Selinger CI, Lyons RJ, Hayes VM, O'Toole SA, Ballinger ML, Gill D, Thomas DM, Mercer TR, Blackburn J: Diagnosis of fusion genes using targeted RNA sequencing. Nat Commun 2019, 10:1388
16. Song W, Platteel I, Suurmeijer AJH, Kempen LC: Diagnostic yield of NanoString nCounter FusionPlex profiling in soft tissue tumors. Genes Chromosomes Cancer 2020, 59:318–324
17. Cheng DT, Mitchell TN, Zehir A, Shah RH, Benayed R, Syed A, Chandramohan R, Liu ZY, Won HH, Scott SN, Brannon AR, O'Reilly C, Sadowska J, Casanova J, Yannes A, Hechtman JF, Yao J, Song W, Ross DS, Oultache A, Dogan S, Borsu L, Hameed M, Nafa K, Arcila ME, Ladanyi M, Berger MF: Memorial Sloan Kettering-integrated mutation profiling of actionable cancer targets (MSK-IMPACT). J Mol Diagn 2015, 17:251–264

18. McConnell L, Houghton O, Stewart P, Gazdova J, Srivastava S, Kim C, Catherwood M, Strobl A, Flanagan AM, Oniscu A, Kroeze LI, Groenen P, Taniere P, Salto-Tellez M, Gonzalez D: A novel next generation sequencing approach to improve sarcoma diagnosis. Mod Pathol 2020, 33:1350−1359
19. de Vree PJP, de Wit E, Yilmaz M, van de Heijning M, Klous P, Verstegen MJAM, et al: Targeted sequencing by proximity ligation for comprehensive variant detection and local haplotyping. Nat Biotechnol 2014, 32:1019−1025
20. Troll CJ, Putnam NH, Hartley PD, Rice B, Blanchette M, Siddiqui S, Ganbat J-O, Powers MP, Ramakrishnan R, Kunder CA, Bustamante CD, Zehnder JL, Green RE, Costa HA: Structural variation detection by proximity ligation from formalin-fixed, paraffin-embedded tumor tissue. J Mol Diagn 2019, 21:375−383
21. Simonis M, Klous P, Homminga I, Galjaard R-J, Rijkers E-J, Grosveld F, Meijerink JPP, de Laat W: High-resolution identification of balanced and complex chromosomal rearrangements by 4C technology. Nat Methods 2009, 6:837−842
22. Allahyar A, Pieterse M, Swennenhuis J, Los-de Vries GT, Yilmaz M, Leguit R, Meijers RWJ, van der Geize R, Vermaat J, Cleven A, van Wezel T, Diepstra A, van Kempen LC, Hijmering NJ, Stathi P, Sharma M, Melquiond ASJ, de Vree PJP, Verstegen MJAM, Krijger PHL, Hajo K, Simonis M, Rakszewska A, van Min M, de Jong D, Ylstra B, Feitsma H, Splinter E, de Laat W: Robust detection of translocations in lymphoma FFPE samples using targeted locus capture-based sequencing. Nat Commun 2021, 12:3361
23. Richardson SO, Huibers MMH, de Weger RA, de Leng WWJ, Hinrichs JWJ, Meijers RWJ, Willems SM, Peeters TLMG: One-fits-all pretreatment protocol facilitating fluorescence in situ hybridization on formalin-fixed paraffin-embedded, fresh frozen and cytological slides. Mol Cytogenet 2019, 12:27
24. Agaimy A, Baněčková M, de Almeida J, Dickson BC, Dimmler A, Hartmann W, Laé M, Pablik J, Schubart C, Skálová A, Stoehr R, Trautmann M, Wardelmann E, Wassef M, Weinreb I: Recurrent EWSR1::COLCA2 fusions define a novel sarcoma with spindle/round cell morphology and strong predilection for the sinonasal tract. Am J Surg Pathol 2023, 47:361−369
25. Creytens D, Mentzel T, Ferdinande L, Lecoutere E, van Gorp J, Atanesyan L, de Groot K, Savola S, van Roy N, van Dorpe J, Flucke U: "Atypical" pleomorphic lipomatous tumor. Am J Surg Pathol 2017, 41:1443−1455
26. Racanelli D, Brenca M, Baldazzi D, Goeman F, Casini B, de Angelis B, Guercio M, Milano GM, Tamborini E, Busico A, Dagrada G, Garofalo C, Caruso C, Brunello A, Pignochino Y, Berrino E, Grignani G, Scotlandi K, Parra A, Hattinger CM, Ibrahim T, Mercatali L, de Vita A, Carriero MV, Pallocca M, Loria R, Covello R, Sbaraglia M, Dei Tos AP, Falcioni R, Maestro R: Next-generation sequencing approaches for the identification of pathognomonic fusion transcripts in sarcomas: the experience of the Italian ACC sarcoma working group. Front Oncol 2020, 10:489
27. Rosenberg AR, Skapek SX, Hawkins DS: The inconvenience of convenience cohorts: rhabdomyosarcoma and the PAX-FOXO1 biomarker. Cancer Epidemiol Biomarkers Prev 2012, 21:1012−1018
28. Barr FG, Nauta LE, Davis RJ, Schafer BW, Nycum LM, Biegel JA: In vivo amplification of the PAX3-FKHR and PAX7-FKHR fusion genes in alveolar rhabdomyosarcoma. Hum Mol Genet 1996, 5: 15−21
29. Miquelestorena-Standley E, Jourdan M-L, Collin C, Bouvier C, Larousserie F, Aubert S, Gomez-Brouchet A, Guinebretière J-M, Tallegas M, Brulin B, le Nail L-R, Tallet A, le Loarer F, Massiere J, Galant C, de Pinieux G: Effect of decalcification protocols on immunohistochemistry and molecular analyses of bone samples. Mod Pathol 2020, 33:1505−1517
30. Cohen D, Hondelink LM, Solleveld-Westerink N, Uljee SM, Ruano D, Cleton-Jansen A-M, von der Thüsen JH, Ramai SRS, Postmus PE, Graadt van Roggen JF, Hoppe BPC, Clahsen PC, Maas KW, Ahsmann EJM, ten Heuvel A, Smedts F, van Rossem RN, van Wezel T: Optimizing mutation and fusion detection in NSCLC by sequential DNA and RNA sequencing. J Thorac Oncol 2020, 15:1000−1014